Phosphorus extracted municipal sludge-derived hydrochar as a potential solid fuel: Effects of acidic leaching and combustion mechanism

Huan Liu, Nathalie Lyczko, Ange Nzihou, Cigdem Eskicioglu

Phosphorus extracted municipal sludge-derived hydrochar as a potential solid fuel: Effects of acidic leaching and combustion mechanism

Huan Liu, Nathalie Lyczko, Ange Nzihou, Cigdem Eskicioglu

[a] UBC Bioreactor Technology Group, School of Engineering, The University of British Columbia, Okanagan Campus, 1137 Alumni Avenue, Kelowna, British Columbia V1V 1V7, Canada

[b] Université de Toulouse, IMT Mines Albi, RAPSODEE CNRS UMR 5302, Campus Jarlard, F.81013 Albi Cedex 09, France

[c] Princeton University, School of Engineering and Applied Science, Princeton, NJ 08544, USA

[d] Princeton University, Andlinger Center for Energy and the Environment, Princeton, NJ 08544, USA

Hydrochar from hydrothermal liquefaction (HTL) of municipal sludge is often seen as waste. Initially, acidic leaching has been performed on hydrochar to recover phosphorus. This study evaluated the resulting hydrochar as solid fuel, thus achieving zero waste for integrating HTL into wastewater treatment plants. The effects of various leaching conditions on acid-modified hydrochar properties were examined. Compared to raw hydrochar, acid-modified hydrochar had a significant ash reduction (up to 44%). The leaching conditions (10 mL of 0.6 N HNO_3/g for 2 h) for near-complete phosphorus extraction also achieved the following most desirable properties of acid-modified hydrochar: Maximized fuel ratio (1.3), higher heating value (20.5 MJ/kg), carbon content (48%), and minimized ash content (34%) on a dry basis. By removing most alkali and alkaline earth metals, acid-modified hydrochar could carry a low slagging and fouling risk compared to a high/severe risk for raw hydrochar. Acidic leaching also enhanced ignition temperature from 317 to 351 °C for safer storage and transportation of hydrochar, with a higher comprehensive combustion index (up to 9.9×10^{-8} min^{-2} $°C^{-3}$). Overall, hydrochar fuel property was improved by acid modification, comparable to bituminous coal. For the first time, it was identified that hydrochar combustion was controlled by a two-step n^{th}-order reaction mechanism $f(\alpha) = (1 - \alpha)^n$ with the reaction order changing from 3 to 1 as progressed. The acid modification did not affect combustion mechanisms but reduced activation energy in the first stage. The results demonstrated a sustainable approach for closing the waste loop and provided a pathway for transforming hydrochar into biofuel.

1. Introduction

Hydrothermal liquefaction (HTL) has been found one of the most promising waste-to-energy technologies [1]. It is particularly suitable for treating organic waste with high moisture but low dewaterability, such as municipal sludge (often called sewage sludge) from wastewater treatment plants (WWTPs). HTL uses subcritical water to convert organic fractions (typically 75–85% moisture) into a petroleum-like product (biocrude) at elevated temperatures (280–374 °C) and pressures (8–22 MPa) in a closed system [2]. As a result, it also generates three byproducts: HTL aqueous – process water with dissolved fractions [3], hydrochar – solid residue with most minerals and some organic carbon, and gaseous phase – mainly CO_2. The development of HTL has been focused on the production of renewable energy (biocrude) in the last decade, while the byproducts received much less attention [4]. However, in the circular economy, all waste is treated as a resource instead of a cost, which demands sustainable solutions for the goal of a better environment and economy. Therefore, the valorization of HTL byproducts requires more knowledge to eliminate waste and pollution.

Hydrochar from HTL of municipal sludge is often considered to be disposed of as waste for its small volume (94–99% less than sludge input) [5]. Compared to hydrochar from hydrothermal carbonization (HTC) performed at lower reaction temperatures (180–280 °C), HTL hydrochar is less attractive as a solid fuel for its higher ash contents (mostly > 45%, dry basis – db) and lower calorific values (mostly < 10 MJ/kg, db) [2]. However, recent studies have found that sludge-derived hydrochar could be a secondary phosphorus (P) source for the recovery of fertilizers or other value-added products [6]. For example, hydrochar

from HTL of primary sludge and mixed (primary + secondary) sludge could reach a P content of up to 10% and 8.5%, db, respectively, which is as high as that (around 8%) in low-grade phosphate rock [7,8]. Acidic extraction is found to be the most suitable approach for P recovery from hydrochar due to its high efficiency, simplicity, and relatively low cost [6]. Our previous study has demonstrated that most P can be recovered from hydrochar by nitric acid and turned into a multifunctional hydroxyapatite [9]. On the other hand, acidic leaching is likely to remove ash or minerals from hydrochar and enhances its properties as a solid fuel [10]. The removal of alkali metals by acid washing can also mitigate the slagging and fouling risks in boilers [11]. Consequently, it is worth exploring if an acid modification can improve the desirability of hydrochar for combustion and closed-loop recycling.

To date, limited studies have assessed the effects of acidic leaching on hydrochar properties. Marin-Batista et al. initially confirmed that acidic leaching of HTC hydrochar from digested sludge by 1 N HCl at a liquid-to-solid (L/S) ratio of 50 mL/g for 6 h could reduce the ash contents by around 50% and increase higher heating value (HHV) by 1.5 times [12]. Nzediegwu et al. also found that modification by 20 mL/g of 3.5% nitric acid enhanced fuel properties of HTC hydrochar while the effects depended on feedstock type [10]. However, another study using 5% organic acids (citric, oxalic, and tartaric acid) only slightly increased HHVs by 1.1 times of sludge-derived HTC hydrochar, although most P was extracted [13]. This suggests that more comprehensive investigations are required to validate whether desirable solid fuel can be produced after P recovery. It is also necessary to gain a more in-depth understanding of how acid modification (e.g., different leaching conditions) affects hydrochar characteristics and combustion performance.

Besides improving fuel properties, uncovering the combustion kinetics of hydrochar is an essential step for process optimization. Kinetic parameters need to be properly estimated for simulating computational fluid dynamics and supporting combustor design and maintenance [14]. Thermogravimetry analysis (TGA) is a commonly used approach that can quickly describe thermal degradation behaviors and kinetics. However, without knowing the mechanism, most studies used model-free isoconversional methods such as Friedman, Kissinger-Akahira-Sunose (KAS), and Ozawa-Flynn-Wallt to calculate activated energy (E) from non-isothermal TGA data by treating the whole decomposition process as a single step [15,16]. This is the simplest approach, but it does not give other kinetic parameters, i.e., pre-exponential factor (A) and reaction model f(α). The others employed the model-fitting method (e.g., Coats-Redfern) by assuming that hydrochar combustion followed an order-based reaction model [17,18]. These methods cannot clearly identify the combustion mechanism or may lead to physical ambiguities because hydrochar combustion is often complex and composed of parallel reactions that require deconvolution to interpret individual steps [19]. Therefore, applying the multi-step kinetics is critical for properly identifying the kinetic triplets (E, A, and f(α)) of hydrochar combustion and filling the research gaps.

This study aims to evaluate the feasibility of using modified hydrochar (MHC) as a solid fuel after P extraction by acid to close the waste loop in HTL processing of waste municipal sludge. Firstly, the effects of acidic leaching conditions on hydrochar properties were examined. Secondly, the potential slagging and fouling risks of hydrochar before and after acidic leaching were assessed using various indices. Thirdly, the combustion behaviors of raw and modified hydrochar were illustrated by a non-isothermal TGA. Lastly, combustion mechanisms were exposed using multi-step models, as compared to single-step kinetics. Consequently, the impacts of acid modification on hydrochar combustion kinetics could be discovered.

2. Materials and methods

2.1. Materials

Hydrochar (HC) was obtained as described previously after HTL (350 °C for a residence time of 15 min) of dewatered (20% solids by weight) municipal mixed sludge, comprised of primary and secondary sludge [9,20]. The mixed sludge was obtained from a local WWTP in BC, Canada, which has primary and two-stage secondary (biological) treatment processes (trickling filters followed by solid-contact tanks). Acidic leaching was applied to hydrochar to extract P at various conditions: L/S ratio (5–100 mL/g), nitric acid concentration (0.02–1 N), and contact time (0–24 h) [9]. Subsequently, the MHC was neutralized (washed with 1 L deionized water), collected, dried at 105 °C for 24 h, and stored at 4 °C before analysis.

2.2. Characterization of hydrochar

Dried hydrochar samples were characterized to reveal their fuel properties. The proximate analysis (ash and volatile matter) was conducted according to ISO Methods 18122 and 18123, while fixed carbon was estimated from the difference (%fixed carbon = 100 – %ash – % volatile matter). Fuel ratio was expressed by the content ratio of fixed carbon over volatile matter.

An automatic elemental analyzer (Thermo Scientific™ Flash 2000) was employed for ultimate analysis (CHNS), and O content was calculated from the difference (O% = 100 – %CHNS – %ash). The determination of CHNS was by the complete combustion at 950 °C using pure oxygen (99.95%) and converting CHNS into CO_2, H_2O, N_2, and SO_2, respectively. The converted gas was subsequently separated by a GC column and quantified by a thermal conductivity detector. The analyzer was calibrated before analysis using methionine standard (Elemental Microanalysis) with an accuracy of ± 2% for CHNS. Each time, 1–3 mg of powder hydrochar was wrapped in a small tin container and loaded for analysis. Samples were measured in triplicates and standard errors were shown as error bars in figures.

A bomb calorimeter (IKA® C5000) was used to determine HHV. Before analysis, the calibration was performed with a calorimetric standard – benzoic acid tablet (NIST39J, IKA) under 30 bars of pure oxygen (99.95%) at 22 °C. The relative standard deviation (6 replicates) was found within 0.1% of the theoretical number. Each time, 0.3–0.5 g of hydrochar sample was pressed into a pellet for HHV analysis. A duplicate analysis of each sample was conducted.

An X-ray fluorescence (XRF) analyzer (Malvern Panalytical Epsilon3-XL) was employed to measure mineral contents (Fe_2O_3, CaO, MgO, Na_2O, K_2O, SiO_2, Al_2O_3, and TiO_2) in semi-quantitative mode with an accuracy of ± 10%. Calibration for this method was completed by the supplier. For analysis, approximately 5 g of powder samples were transferred to the sample holders. After measurement, the matrix composition (CHNSO content) was specified for each sample, and mineral contents were automatically calculated by the Omnian program. Each analysis was repeated threefold with the average reported and relative standard deviations from duplicate runs were < 4%. Detailed procedures of the above analyses can be found in Chapter 2 of the Handbook on Characterization of Biomass, Biowaste and Related By-products [21].

2.3. Slagging and fouling indices

The presence of minerals/ash in hydrochar could cause slagging and fouling issues during combustion. Slagging is caused by the deposition of molten ash on heat-transfer surfaces mainly exposed to radiant heat, while fouling defines the deposits of fly ash (quenched below the melting point), condensation of volatiles, or sulfidation by SO_3 in the heat recovery section of a boiler [22]. Various indices (Table 1) have been established to predict the likelihood of slagging and/or fouling by considering the dry contents of minerals.

Alkali metals in fuel could vaporize during combustion in a boiler and then condense and deposit alkali matrix on heat transfer surfaces [24]. The alkali index (AI) was developed by the coal industry by calculating alkali oxides ($Na_2O + K_2O$) per heat unit, kg/GJ in the fuel to

Table 1
Empirical indicators for the prediction of slagging and fouling potential [11,23–27].

Indicator	Equation[b]	Slagging and/or fouling risk			
		Low	Medium	High	Severe
Alkali index (AI)	$AI(kg/GJ) = \frac{Na_2O+K_2O}{HHV(GJ/kg)}$	<0.17	0.17–0.34	>0.34	–
Base-to-acid ratio (B/A)	$B/A = \frac{Fe_2O_3 + CaO + MgO + Na_2O + K_2O + (P_2O_5)}{Al_2O_3 + SiO_2 + TiO_2}$	–			
Slagging index (SI)[a]	$SI = B/A \times S\%$	<0.6	0.6–2.0	2.0–2.6	>2.6
Fouling index (FI)[a]	$FI = B/A \times (Na_2O\% + K_2O\%)$	<0.2	0.2–0.5	0.5–1.0	>1.0
Slag viscosity index (SVI)	$SVI = \frac{SiO_2}{SiO_2 + Fe_2O_3 + CaO + MgO} \times 100$	>72	65–72	<65	–

[a] Only applicable to bituminous ashes, when $Fe_2O_3\% > CaO\% + MgO\%$.
[b] HHV – higher heating value (dry basis).

classify slagging and fouling propensities based on plant experience and field tests [23].

The ash typically contains basic (Fe_2O_3, CaO, MgO, Na_2O, and K_2O) and acidic (SiO_2, Al_2O_3, and TiO_2) oxides, which have lower and higher melting points, respectively [26]. In addition, a considerable fraction of P_2O_5 could increase low-melting-point phases in fly ash and therefore can be included in the basic group [27]. The base-to-acid ratio (B/A) reflects ash melting potential and relation to slag viscosities and ash fusion temperatures [24]. However, it is not meant to be a single parameter to rate the ash deposition tendency. In the presence of sulfur, slagging index (SI) predicts the propensity of fused slag deposits formed on furnace walls primarily subjected to radiant heat [24]. Incorporating alkali contents, the fouling index (FI) relates to the potential of alkali-bonded deposits formed on convective surfaces [11].

The slag viscosity index (SVI) defines the percentage of silica present in the metal oxides [26]. A high SVI value means a high viscosity and thus a low slagging tendency inside the furnace.

2.4. Combustion performance

The combustion behaviors of selected hydrochar samples were analyzed by simultaneous thermogravimetric analysis and differential thermal calorimetry (TGA–DSC, TA Instruments SDT Q600). Approximately 10 mg sample was placed in a platinum crucible and heated from 30 to 700 °C under an air environment (100 mL/min) at different heating rates (2, 5, and 10 °C/min). Blank experiments for each heating rate were performed using the same empty crucible to correct experimental data. For each batch of analysis, a randomly selected sample was remeasured to ensure repeatability and accuracy.

From TGA and derivative thermogravimetric (DTG) curves, the maximum combustion rate temperature (T_m, °C), maximum mass loss rate (DTG_{max}, %/min), average mass loss (DTG_{mean}, %/min), ignition temperature (T_i, °C), and burnout temperature (T_b, °C) were obtained as previously defined [8]. The combustion performance was compared by the comprehensive combustion index (S, min^{-2} $°C^{-3}$) using Eq. (1).

$$S = \frac{DTG_{max} DTG_{mean}}{T_i^2 T_b} \tag{1}$$

2.5. Combustion kinetics

2.5.1. Single-step kinetics

The kinetics of hydrochar combustion were determined using TGA data. Firstly, the degree of conversion of a material is expressed as a function of temperature by Eq. (2) [28].

$$\alpha = \frac{m_0 - m}{m_0 - m_f} \tag{2}$$

where m_0, m, and m_f are the initial mass (mg, after moisture correction at 150 °C), current mass (mg) at a given temperature T, and final mass (mg) at the end of combustion, respectively.

For reaction controlled by a single step, the rate of solid-state reaction ($d\alpha/dt$ or $d\alpha/dT$) is described by the reaction model function $f(\alpha)$ and Arrhenius equation $k(T)$ as shown in Eqs. (3) and (4), which can be rearranged into Eq. (5). Most common reaction mechanisms and their integral form g(α) are listed in Table S1.

$$\frac{d\alpha}{dt} = k(T) f(\alpha) \tag{3}$$

$$k(T) = A\exp\left(-\frac{E}{RT}\right) \tag{4}$$

$$\frac{d\alpha}{dT} = \frac{A}{\beta} exp\left(-\frac{E}{RT}\right) f(\alpha) \tag{5}$$

where A is the pre-exponential or frequency factor (min^{-1}); E is the activation energy (J/mol); T is the absolute temperature (K); R is the universal gas constant (8.314 J/mol K); and $\beta = dT/dt$ is the heating rate (K/min or °C/min).

Assuming the reaction rate at a constant conversion degree is only a function of temperature, three model-free isoconversional methods in Eqs. (6)–(8) were recommended by International Confederation for Thermal Analysis and Calorimetry (ICTAC) for their accuracy in estimating activation energy without knowing the reaction mechanism [29]. The Friedman method is a differential approach without mathematical approximations, whereas KAS and Starink equations employ a range of approximations for the temperature integral. The differential method is sensitive to baselines of thermal analysis data while integral methods vary based on their type of approximation, and thus they are often used together as complementary to each other [30].

$$\text{Friedman}: \ ln\left(\beta \frac{d\alpha}{dT}\right) = ln[A_\alpha f(\alpha)] - \frac{E_\alpha}{R}\frac{1}{T_\alpha} \tag{6}$$

$$\text{KAS}: \ \ln\left(\frac{\beta}{T_\alpha^2}\right) = \ln\left[\frac{A_\alpha R}{E_\alpha g(\alpha)}\right] - \frac{E_\alpha}{R}\frac{1}{T_\alpha} \tag{7}$$

$$\text{Starink}: \ \ln\left(\frac{\beta}{T_\alpha^{1.92}}\right) = \ln\left[\frac{A_\alpha R^{0.92}}{E_\alpha^{0.92} g(\alpha)}\right] - 0.312 - 1.0008\frac{E_\alpha}{R}\frac{1}{T_\alpha} \tag{8}$$

where E_α, A_α, and T_α are defined the same as above, indicating values at a given α (0.1–0.9).

By linearly fitting the left side of the above equations vs $1/T_\alpha$ at different heating rates, apparent activation energy (E_α) can be determined from the slope of the Arrhenius plot at each α.

2.5.2. Multi-step kinetics

Thermal decomposition of hydrochar is a complex process, often composed of multiple steps with several peaks observed in DTG and DSC curves. Considering the main components of volatile matter and fixed carbon, hydrochar combustion can be described using a two-step parallel reaction model, assuming each component reacts independently [21,31]. It should be noted that more parallel steps may be identified

depending on the reaction complexity [19]. The global reaction rate is written as the sum of the reaction rate of each pseudo-component (PC) i as displayed in Eq. (9).

$$\frac{d\alpha}{dT} = \sum_{i=1}^{j} \left.\frac{d\alpha}{dT}\right|_i \tag{9}$$

where j is the total number of parallel steps, here $j = 2$.

To model parallel reactions, peak deconvolution of reaction rate curves was performed to separate the overlapped PC profiles using statistical functions. Since kinetic curves are often asymmetrical, conventional functions such as Lorentzian and Gaussian without an asymmetry factor are inadequate for deconvolution [32]. Therefore, Fraser-Suzuki algorithm in Eq. (10) that allows asymmetric functions was selected to properly fit kinetic curves.

$$\left.\frac{d\alpha}{dT}\right|_i = H_i exp\left\{ -ln2\left[\frac{\ln(1+2A_{s,i}\frac{T-P_i}{W_i})}{A_{s,i}}\right]^2\right\} \tag{10}$$

where T is the reaction temperature (°C or K), and H_i, $A_{s,i}$, P_i, and W_i are the height (1/°C or 1/K), asymmetry (dimensionless), peak temperature (°C or K), and halfwidth (°C or K) of the curve PC i, respectively.

A computer program (Fityk 1.3.1, LogNormal function) was used for the nonlinear least-squares curve fitting and minimizing fit error as determined by Eq. (11) [28,33].

$$Fit\ error(\%) = \frac{\sqrt{\sum_{k=1}^{N}\left[\left(\frac{d\alpha}{dT}\right)_{exp,\ k} - \left(\frac{d\alpha}{dT}\right)_{cal,\ k}\right]^2}}{\sqrt{N}\left(\frac{d\alpha}{dT}\right)_{exp,\ max}} \times 100 \tag{11}$$

where $(d\alpha/dT)_{exp}$ and $(d\alpha/dT)_{cal}$ are the experimental and calculated values of reaction rate, and N is the number of data points.

Once each parallel reaction is identified, E_α can be calculated using Freidman method in Eq. (6). Subsequently, the most suitable reaction mechanism can be acquired using generalized master plots that only depend on the reaction model f(α) [21]. The generalized master plots can be obtained using the reduced-generalized reaction rate $\lambda(\alpha)$ after normalization by taking $\alpha = 0.5$ as the reference reaction extent, expressed in Eq. (12). The best-fit $f(\alpha)$ can be identified from the best match of experimental $\lambda(\alpha)$ values with the theoretical curves shown in Fig. S1. The overall process of multi-step kinetic analysis is summarized in Fig. 1.

$$\lambda(\alpha) = \frac{f(\alpha)}{f(\alpha)_{\alpha=0.5}} = \frac{(d\alpha/dT)_\alpha}{(d\alpha/dT)_{\alpha=0.5}} \frac{\exp(E_\alpha/RT_\alpha)}{\exp(E_\alpha/RT_\alpha)_{\alpha=0.5}} \tag{12}$$

3. Results and discussion

3.1. Effects of acidic leaching on hydrochar properties

The proximate analysis of solid fuel gives the basis of combustion characteristics, showing the percentage of a material that burns in the gaseous phase (volatile matter) and solid phase (fixed carbon), and combustion residue (ash). Fig. 2 presents the effects of various acidic leaching conditions on proximate analysis of hydrochar. The L/S ratio generally did not have significant effects until it increased to 20 mL/g using 0.1 N HNO_3 for 24 h (Table S2). At an L/S ratio of 20–100 mL/g, acidic leaching significantly ($p < 0.05$) improved volatile matter and fixed carbon by up to 1.15 and 2.19 times, respectively, while reducing ash content by 39% (Fig. 2a). As a result of the changes of volatile matter and fixed carbon, fuel ratio significantly increased for the whole L/S ratio range (5–100 mL/g), from 0.6 to up to 1.1. The HHV showed a similar trend to proximate analysis and started drastically improving at 20 mL/g (Fig. 2b). Regarding the effects of acid concentration by 10 mL/g of HNO_3 for 24 h, significant improvements on volatile matter, fix carbon, fuel ratio, and HHV were found during the range of 0.1–0.6 N,

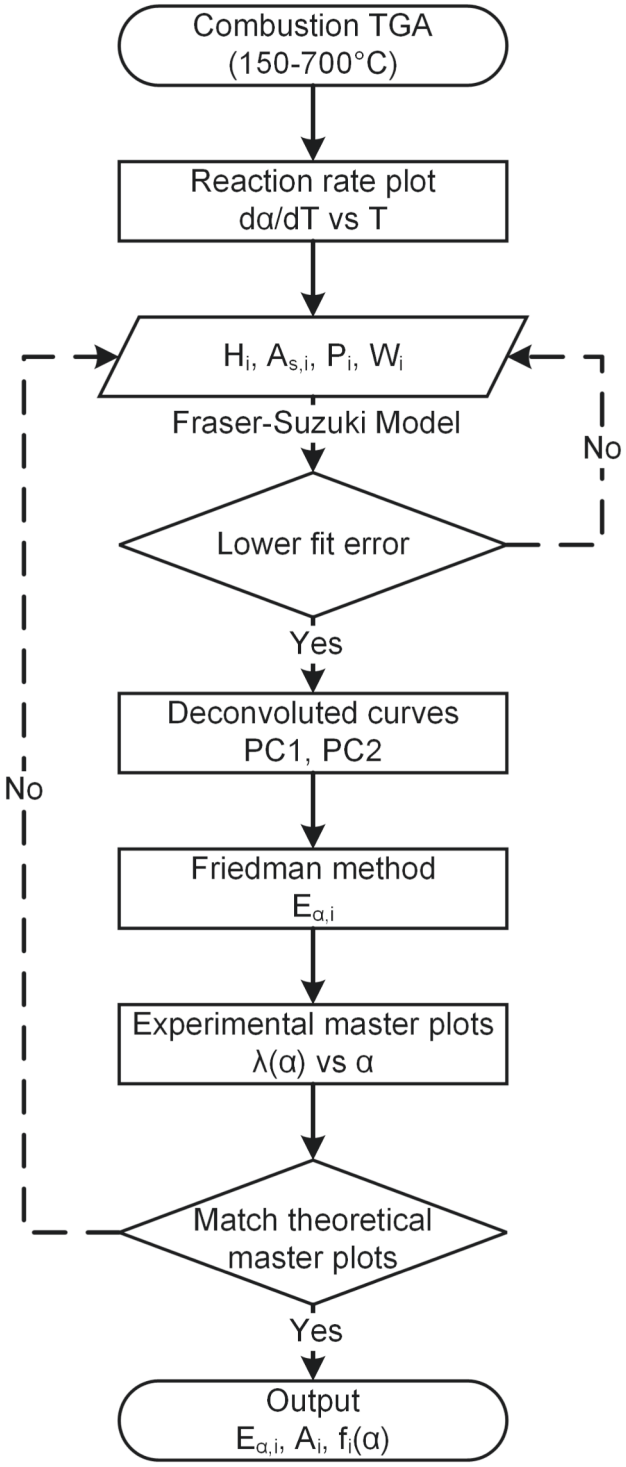

Fig. 1. Flow chart of multi-step kinetic analysis of hydrochar combustion.

with the removal of ash (Fig. 2c-d). However, above 0.6 N, equilibrium was achieved with no significant changes in those properties. Similar effects on proximate analysis of sludge-derived hydrochar were also observed by using more oxalic acid (0.5–5% by weight) for leaching [13]. For contact time, most fuel properties of hydrochar were significantly enhanced within 2 h by 10 mL/g of 0.6 N HNO_3 and generally reached a plateau afterward (Fig. 2e-f). Interestingly, the fuel ratio and HHV of MHC showed a strong correlation (adjusted $R^2 = 0.96$, $p < 0.001$), suggesting that proximate analysis can be used to predict HHV of hydrochar [34]. Overall, acidic leaching could nearly double fixed

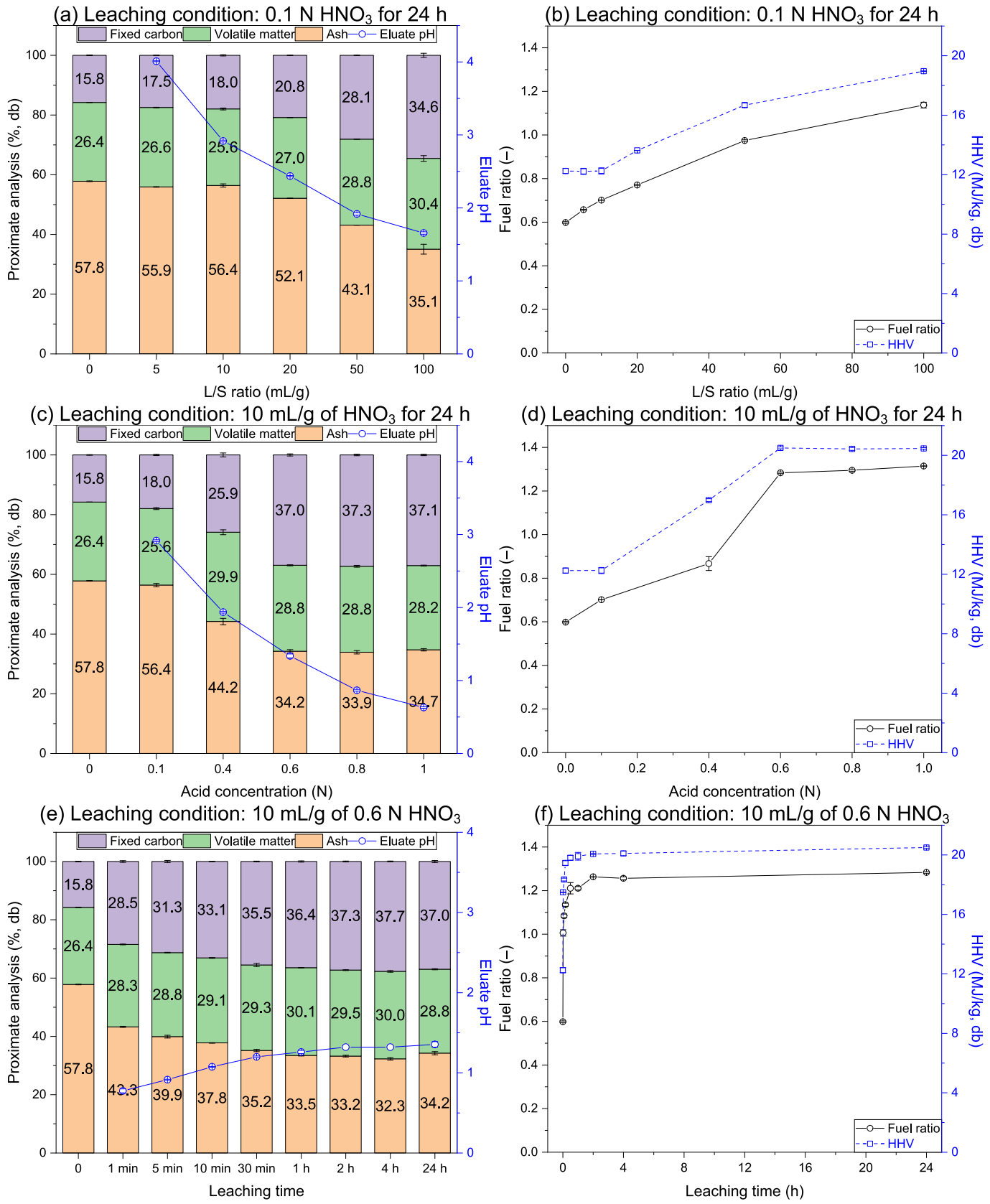

Fig. 2. Effects of (a-b) L/S ratio, (c-d) acid concentration, and (e-f) leaching time on the proximate analysis, fuel ratio, and higher heating value (HHV) of hydrochar on a dry basis (db). Data at x = 0 indicates raw hydrochar.

carbon, fuel ratio, and HHV of MHC compared to raw hydrochar, achieving a comparable quality to bituminous coal [35].

The ultimate analysis represents the major organic elemental composition of hydrochar that reports total CHNS. Fig. 3 illustrates the effects of acid washing on ultimate analysis of hydrochar. It was found that acidic leaching at an L/S ratio of 5 mL/g could significantly increase CHN and increasing L/S ratio did not further change CHN until it went above 20 mL/g (Fig. 3a). Acid concentration at 0.1–0.6 N showed significant positive effects on CHN, while at > 0.6 N there was no further enhancement (Fig. 3c). Likewise, leaching time within 10 min significantly increased CHN but generally reached the maximum at a longer time (Fig. 3e). Notably, different levels of L/S ratio and acid

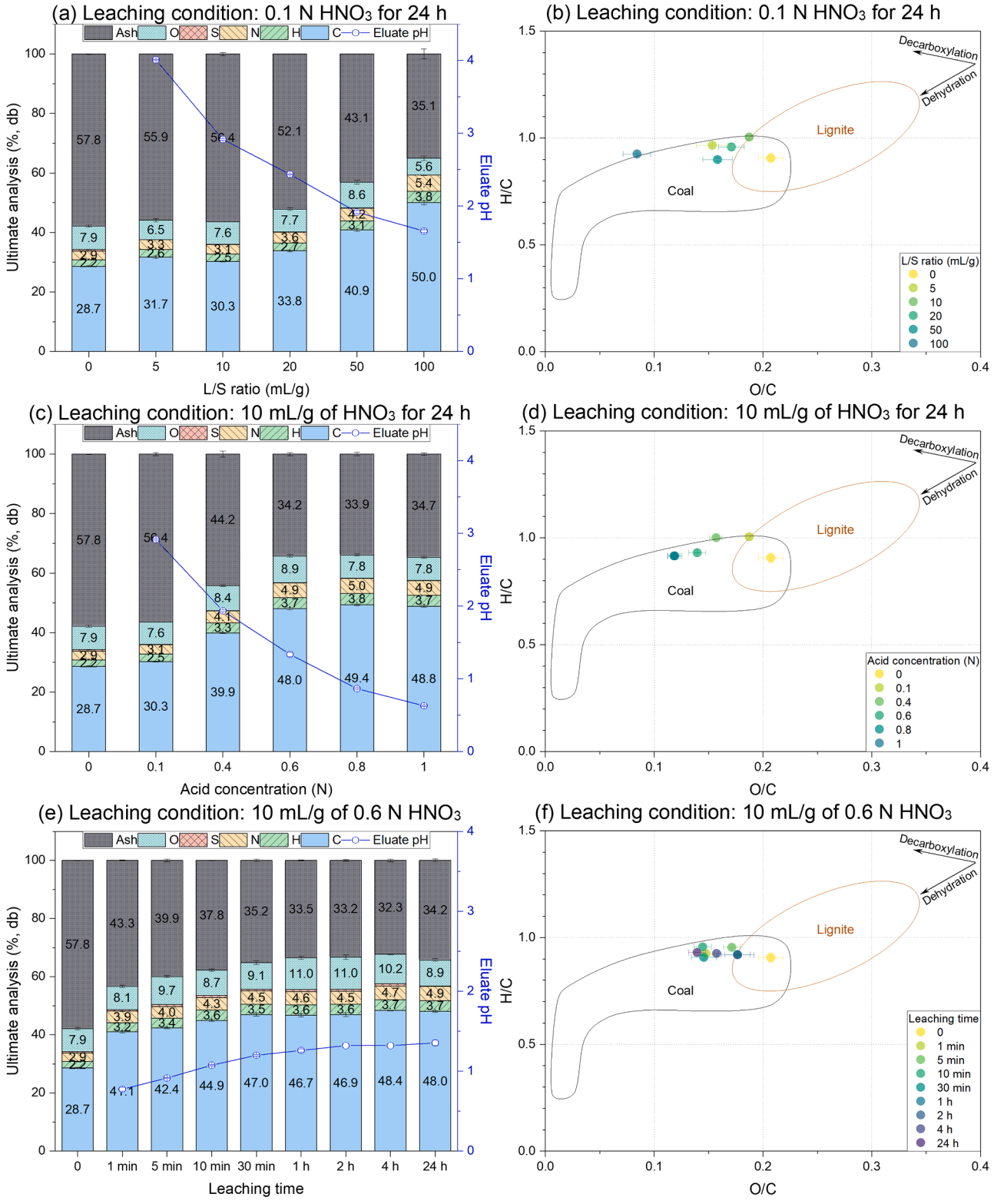

Fig. 3. Effects of (a-b) L/S ratio, (c-d) acid concentration, and (e-f) leaching time on the ultimate analysis on a dry basis (db) and van Krevelen diagram (H/C vs O/C atomic ratios) of hydrochar. Data at x = 0 indicates raw hydrochar.

concentration showed no influence on S contents, while a long leaching time (24 h) significantly decreased S (Table S2). Also, there was no clear effect on O contents, which was probably the combined result of ash and O groups (e.g., carbonates, oxides, and sulfates) removal by acids. The van Krevelen diagrams (Fig. 3b d f) were plotted to reveal conversion reactions during acid treatment of hydrochar. All MHCs had an atomic O/C ratio much lower than that of raw hydrochar while atomic H/C maintained the same level or slightly above the origin. The changes in O/C vs H/C suggested both dehydration and decarboxylation reactions happened during acid treatment. It has been reported that acid-washing biochar can promote dehydration reactions by converting alcohols to ethers and alkenes (losing O as H_2O) and accelerate decarboxylation reactions of O-rich organics (removing O as CO_2) [36]. The O/C ratio can also be reduced by removing carbonates, hydroxides, and oxygenated organic compounds (e.g., acids and phenols) [12]. The leaching variables (L/S, concentration, and time) all showed positive effects on dehydration and decarboxylation reactions, while some variations were likely caused by the competition between hydration and dehydration reactions [10]. Generally, acid washing could improve CHN contents by over 1.6 times than those of raw hydrochar and upgrade the fuel quality towards higher-grade coal by removing oxygenated compounds.

One consistent finding for the effects of L/S ratio and acid concentration was that there was no significant change in hydrochar properties until the eluate pH from acidic leaching reached < 3, indicating that sufficient free acids are necessary for improving fuel quality. The results agreed that the best fuel quality could be achieved by leaching with 10 mL/g of 0.6 N HNO_3 within 2 h, where most P can be recovered as previously reported [9]. However, a long leaching time (24 h) was beneficial for the removal of S that can be reduced from 0.5%, db in raw hydrochar to around 0.1%, db. The linear increase of fuel ratio and HHV in terms of P leaching efficiency (Fig. S2) also indicated that recovering P by acidic leaching can simultaneously improve fuel properties of hydrochar for reuse.

A Pearson correlation analysis was performed by OriginPro 2023 (OriginLab Corp.) to examine the correlation between hydrochar properties due to acid modification. Based on the correlation coefficient plot (Fig. 4), volatile matter, fixed carbon, fuel ratio, HHV, and CHN contents all showed a strong positive correlation to each other ($r > 0.7$, $p < 0.05$), while they were all negatively correlated to ash content ($r < -0.8$, $p < 0.05$). The significant correlations suggested that the improvement of hydrochar fuel properties was probably related to the removal of ash by acidic leaching. Similar conclusions were also drawn for leaching of digested sludge-derived hydrochar by excessive HCl [12]. To normalize the influences of ash reduction due to acid treatment, the dry ash-free (daf) contents of all other parameters were calculated and compared (Fig. S3) to show the individual effects of acid leaching, which presented a different trend from dry-basis contents in Fig. 3. All leaching factors (L/S, concentration, and time) showed significant negative effects on dry ash-free volatile matter (Fig. S3a c e), indicating that acid also removed some volatile matter (<15%, daf). However, they had limited impacts on dry ash-free ultimate analysis (Fig. S3b d f), and only excessive acids (e.g., eluate pH < 2 at a high L/S ratio or acid concentration) significantly increased CHN and reduced O. As shown in Fig. S3b-f, at an L/S ratio of 10 mL/g, a higher acid concentration (>0.6 N) or longer leaching time (>2h) did not significantly change the ash-free content of proximate and ultimate analyses, indicating that the leaching conditions (10 mL/g of 0.6 N HNO_3 for 2 h) maximized MHC properties. Compared to Song et al. using oxalic acid ($Ka_1 = 5.9 \times 10^{-2}$) [13], nitric acid ($K_a = 24$) in this study is much stronger that can simultaneously extract P and remove most minerals, whereas oxalic acid can form insoluble calcium oxalate that would likely retain in MHC and thus limit its property [6]. The enhancement of hydrochar properties by acidic leaching can be summarized into two reasons: 1) The removal of ash or minerals increases the organic content and HHV in MHC; and 2)

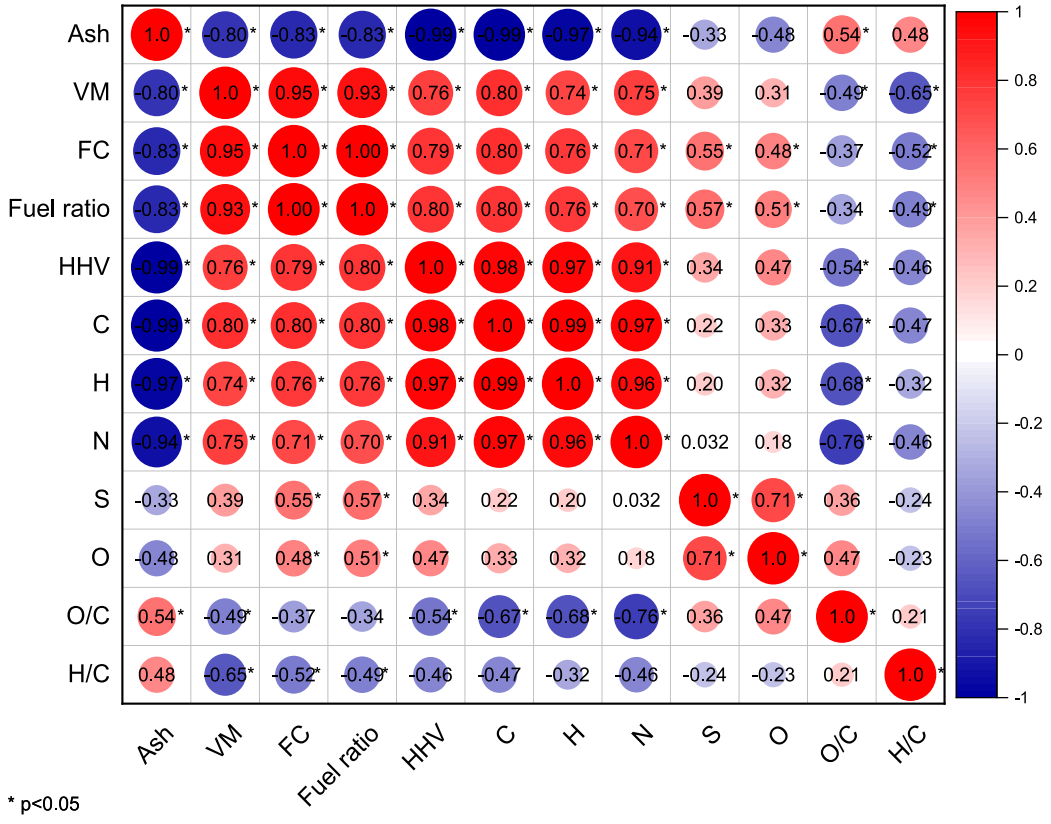

Fig. 4. Pearson correlation plot among properties (dry basis) of hydrochar as a result of acid modification. VM – volatile matter, FC – fixed carbon, HHV = higher heating value.

the loss of oxygen and light volatiles upgrade the fuel quality.

3.2. *Effects of acid leaching on slagging/fouling risks of hydrochar*

Hydrochar contains high ash contents that cause concerns of slagging and fouling problems as a solid biofuel in industrial boilers. However, acidic leaching removes ash and can likely mitigate such issues. Mineral compositions (Table S3) of raw hydrochar and MHC were determined to estimate potential slagging and fouling risks during hydrochar composition. Most minerals (e.g., Na_2O, CaO, MgO, Fe_2O_3, and P_2O_5) in hydrochar clearly declined after acidic leaching with increasing L/S ratio, acid concentration, and/or contact time. After leaching, some minerals (e.g., K_2O, Al_2O_3, and TiO_2) showed limited decreases or even increases at some points, which was probably caused by their acid-insoluble forms, such as K_2SiO_3, $KAlSi_3O_8$, $Ca_2(Fe_{1-x}Al_x)_2O_5$, $MgFeAlO_4$, and rutile (the most common natural form of TiO_2) [37–39]. Silica is generally insoluble in nitric acid and thus SiO_2 was concentrated in modified hydrochar due to the removal of other minerals. The concentrated silicate could be problematic or advantageous during combustion: It can form low-temperature melting eutectics with alkali metals and cause ash fusion (silicate melt-induced slagging) when furnace temperatures are over the melting point; on the other hand, it can also react with other metals (e.g., Ca, Al, and Fe) to form high-temperature melting minerals and enhance ash fusion temperatures [11]. Therefore, potential risks related to silicate were further examined with slagging indices.

Based on the mineral compositions, the slagging and fouling indices can be estimated by equations in Table 1 to evaluate the effects of acidic leaching on slagging and fouling risks during hydrochar combustion. The AI gradually decreased from 0.47 to 0.1 kg/GJ with increasing L/S ratio (Fig. 5a) and acid concentration (Fig. 5b), which maintained a minimum (0.08–0.09 kg/GJ) at $>$ 0.6 N. It also dropped sharply to the lowest level within 10 min of contact time by 10 mL/g of 0.6 N HNO_3 (Fig. 5c). The decrease of AI is due to increased HHV and reduced contents of alkali metals (K and Na) in modified hydrochar, suggesting that acidic could reduce slagging risk from high to low. The SI showed similar decreasing trends (from 1.57 to as low as 0.01) regarding the effects of leaching variables. The reduction of SI is related to decreased B/A (basic oxides removed but acidic oxides remained) and S contents by acid washing, which diminished the slagging risk from medium to low. Contrary to AI and SI, SVI steadily increased from 25% to 71% and 85% with increasing L/S ratio and acid concentration, respectively, and it steeply raised to the highest level (>76%) within 2 h of contact time. The SVI is enhanced by the removal of Ca, Mg, and Fe and concentrated Si in MHC. Its improvement indicated that the slagging risk dropped from high to low. Smith et al. found that secondary sludge-derived hydrochar with a SI of $\leq$ 0.6 and SVI of 80% had high ash fusion temperatures (e.g., 1220–1240 °C of initial deformation temperature), confirming a low slagging potential [40]. In addition, FI greatly declined (>2 folds) until it reached the minimum as L/S ratio, acid concentration, and time increased, implying that the fouling risk was also reduced (from severe to low) after acid treatment due to the removal of alkali, alkaline earth, and transition metals. All indices agreed that the slagging and fouling risks for hydrochar combustion can be minimized to the lowest level through acidic leaching using 10 mL/g of 0.6 N HNO_3 within 2 h. Many studies have found that biowastes (e.g., municipal sludge, greenhouse waste, municipal solid waste, and digestate) and their derived hydrochar can have a high potential of slagging and fouling in combustion, preventing their feasibility as solid fuels [8,40,41]. Nevertheless, this study demonstrates that acidic leaching seems to be a sustainable approach for both resource recovery and fuel quality upgrading. It is recommended that ash fusion tests should be performed for verification when designing a boiler, considering those indices were initially based on coal ash behaviors.

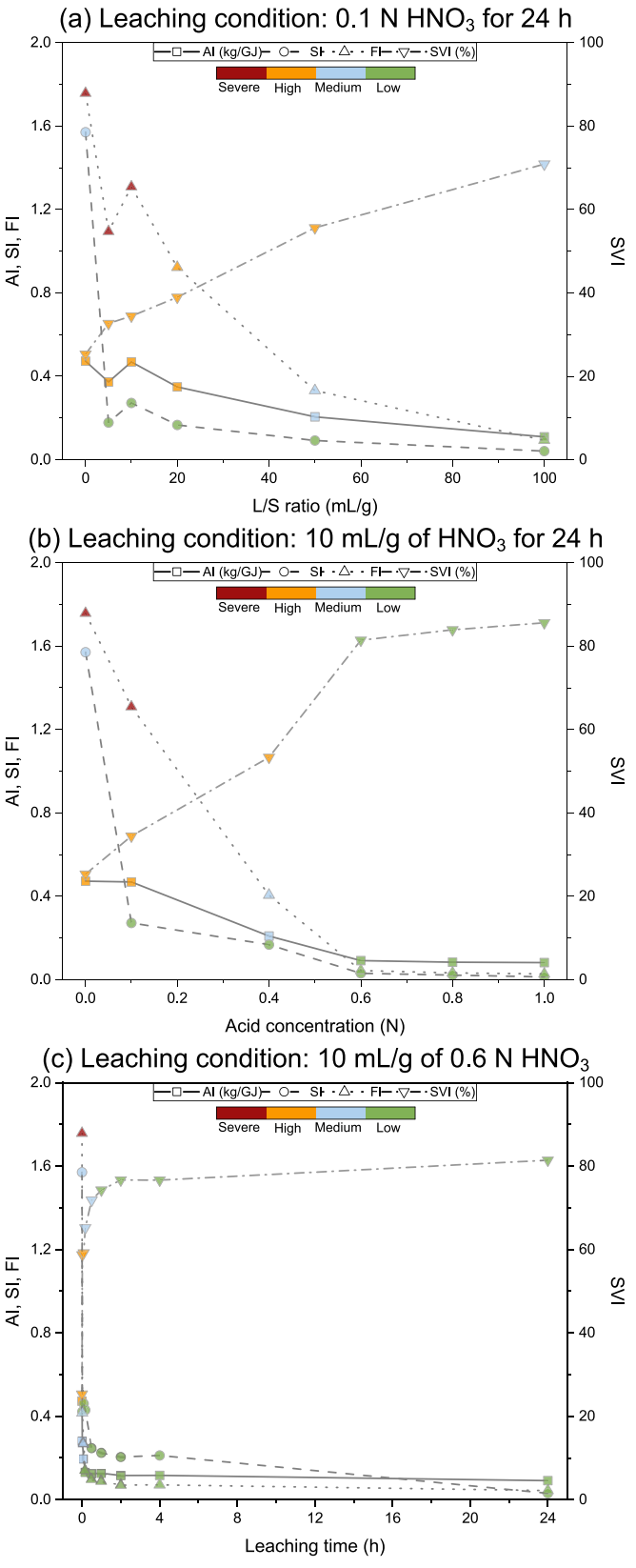

Fig. 5. Effects of (a) L/S ratio, (b) acid concentration, and (c) leaching time on the slagging and fouling risks of hydrochar during combustion. Symbol color indicates risk level of slagging and fouling. Data at x = 0 indicates raw hydrochar. AI – alkali index, SI – slagging index, FI – fouling index, SVI – slag viscosity index.

3.3. Effects of acid leaching on combustion characteristics of hydrochar

The combustion behaviors of hydrochar and modified hydrochar from different acid concentrations were compared by TGA-DSC curves (Fig. 6). Though only one major peak was displayed in DTG curves, the two exothermic peaks in DSC curves suggested two oxidation stages during hydrochar combustion. As previously reported, hydrochar combustion can be generally divided into three steps: (1) Dehydration (30–150 °C), (2) devolatilization (150–330 °C), and (3) char combustion (330–600 °C) [8]. Compared to raw hydrochar, modified hydrochar after acidic leaching showed an elevated weight loss rate (DTG) and heat flow (DSC), leaving less residue (ash) after combustion. Hydrochar modified at higher acid concentrations also had higher DTG and DSC peaks, and the elevation was more noticeable in the char combustion stage which was related to the increase of fixed carbon. The TGA-DTG curves (Fig. 6a c) obtained at different heating rates (taking 2 and 10 °C/min as examples) were generally consistent, while heat flow values (Fig. 6b d) raised with increasing heating rate since energy was released in a shorter time.

Some parameters were estimated to evaluate the combustion characteristics using TGA data from 10 °C/min (Table 2). The ignition and burnout temperatures were determined by the intersection method as shown in Fig. S4. The ignition temperature of hydrochar was generally high (≥317 °C) that increased to up to 351 °C by acidic leaching. The ignition temperatures of hydrochar in this study were generally higher than that of biomass, municipal sludge, and hydrochar obtained from lower hydrochar temperatures (e.g., <325 °C), probably due to less volatiles and more fixed carbon [8,42]. The enhanced ignition temperature could also be related to the removal of minerals since Fe_2O_3 and $Fe_3(PO_4)_2$ can catalyze the ignition process [43]. MHC also showed an ignition temperature close to coal (360 °C), suggesting a good alternative solid fuel with low concerns about safety in storage and handling [44]. The burnout temperature did not change dramatically from acid treatment and remained at 489–499 °C, which is also similar to coal (504 °C) [44]. The peak temperature and maximum and average combustion rates of hydrochar also increased due to acidic leaching. As a result, the comprehensive combustion index (S) improved from 3.8 to 9.9 × 10^{-8} min^{-2} $°C^{-3}$, comparable to bituminous coal (7.8 × 10^{-8} min^{-2} $°C^{-3}$), implying enhanced combustion performance [45]. Overall, acidic leaching can improve the combustion characteristics of hydrochar toward coal.

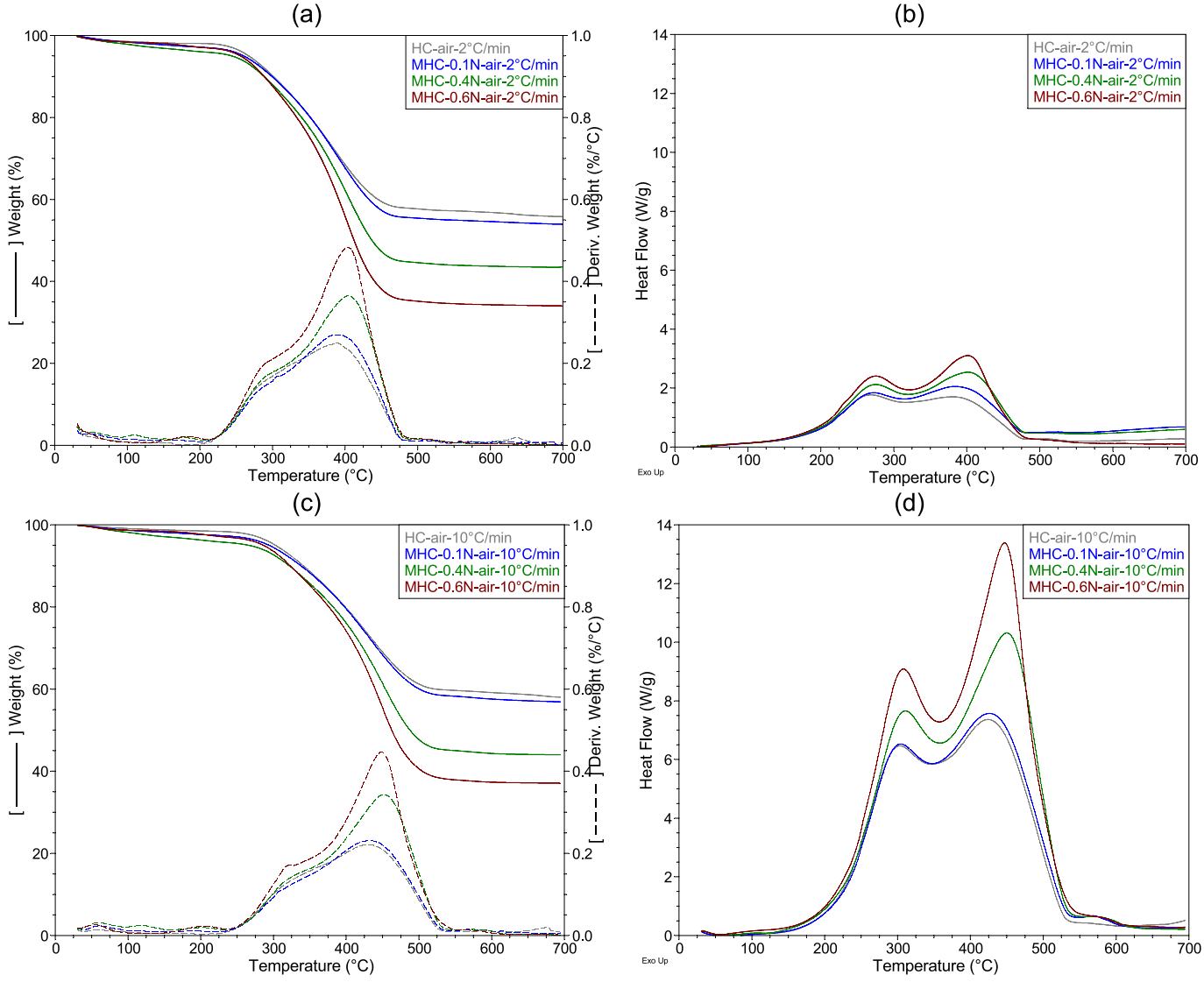

Fig. 6. Thermogravimetric–derivative thermogravimetric (TGA–DTG) and differential thermal calorimetry (DSC) curves of hydrochar (HC) and modified hydrochar (MHC) at a heating rate of (a-b) 2 °C/min and (c-d) 10 °C/min under air environment. Line type follows Y-axis. Line color donates sample. Acidic leaching conditions for MHC are shown in Table 2.

Table 2
Combustion characteristics of raw hydrochar (HC) and modified hydrochar (MHC) obtained from TGA and DTG curves at a heating rate of 10 °C/min.

Sample	Acidic leaching conditions	Ignition temperature T_i (°C)	Peak temperature T_m (°C)	Burnout temperature T_b (°C)	Burnout residue (%)	DTG_{max} (%/min)	DTG_{mean} (%/min)	S ($\times 10^{-8}$ min^{-2} $°C^{-3}$)
HC	–	317	427	489	60.2	2.18	0.87	3.8
MHC-0.1 N	10 mL/g 0.1 N HNO_3 for 24 h	326	429	494	58.2	2.28	0.90	3.9
MHC-0.4 N	10 mL/g 0.4 N HNO_3 for 24 h	351	449	499	44.6	3.39	1.18	6.5
MHC-0.6 N	10 mL/g 0.6 N HNO_3 for 24 h	351	444	490	37.6	4.39	1.36	9.9

3.4. Hydrochar combustion kinetics

3.4.1. Single-step kinetics

The model-free methods Friedman, KAS, and Starink were used to calculate the apparent activation energy (E_α) for hydrochar combustion. Based on TGA data obtained at 2, 5, and 10 °C/min, E_α values at conversion degrees (α) of 0.1–0.9 were estimated (Fig. 7). The linear fitting showed good correlation coefficients ($R^2 = 0.98–1.00$), confirming the reliability of all three methods for describing the combustion process of hydrochar and MHC (Table S4). Due to different mathematical approximations, E_α calculated by the three methods showed small variations but generally give the same trends [28]. Moreover, for each sample, no significant difference ($p > 0.05$) was found in mean E_α values estimated by the three methods, indicating the cross-validation of results from model-free methods. The acidic leaching did not significantly change ($p > 0.05$) mean E_α values and thus not affect the overall kinetics. The average E_α of hydrochar and modified hydrochar was within the range of 130–140 kJ/mol, comparable to that of sewage sludge and its derived hydrochar [15]. The activation energy relates to the difficulty of combustion process of hydrochar, which falls in the range of coal

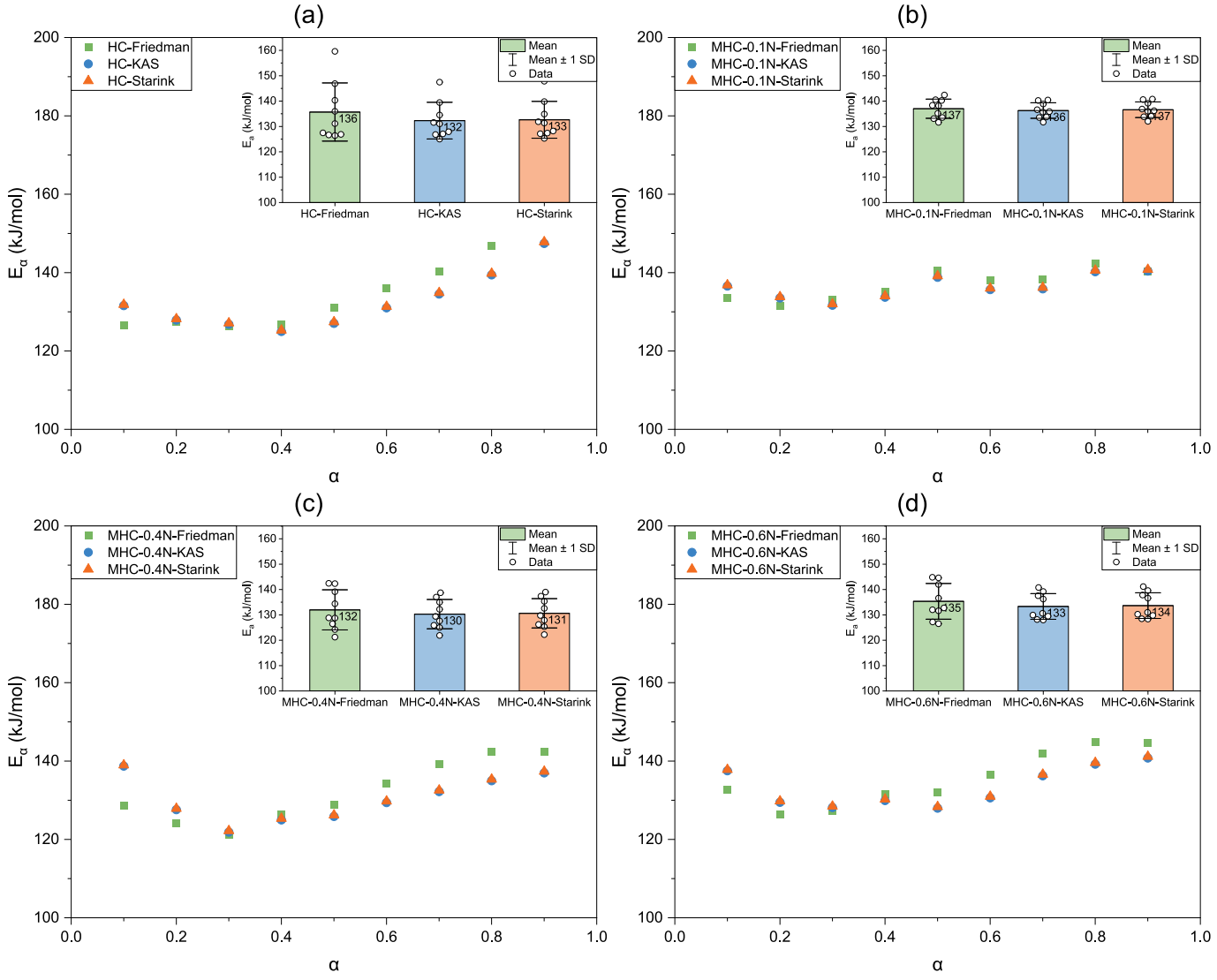

Fig. 7. Estimated apparent activation energy (E_α) in terms of conversion degree (α) by single-step kinetics for combustion of (a) raw hydrochar (HC) and modified hydrochar (MHC) by an acid concentration of (b) 0.1 N, (c) 0.4 N, and (d) 0.6 N. Inset shows a bar chart with mean $E_\alpha \pm$ standard deviation (SD) from each iso-conversional method.

(80–170 kJ/mol) [46].

Practically, a process can be described by single-step kinetics if the uncertainties of E_α are within 10–20% [47]. Although the relative standard deviation from each test was within 2–8% of the mean E_α, differences between the minimum and maximum E_α were up to 24% of the average E_α. The large fluctuations implied that the combustion process of hydrochar was likely dominated by more than one step and thus cannot be simply described by single-step kinetics. Moreover, E_α showed a clear dependence on α, which generally decreased at α of 0.1–0.4 and increased at $\alpha > 0.4$. This phenomenon suggests two reaction stages during hydrochar combustion: Devolatilization improved surface structure (pores and surface area) and thus decreased E_α over temperature, and fixed carbon combustion with enhanced E_α due to more thermal resistance of fixed carbon and ash [48]. Therefore, it is necessary to separate these two steps and further identify the combustion mechanism (rate-limiting steps) of hydrochar.

3.4.2. *Multi-step kinetics*

The curves of reaction rate (dα/dT) vs temperature of raw hydrochar and modified hydrochar from each heating rate were plotted and overlapped peaks were deconvoluted into two major pseudo-component (PCs) using Fraser Suzuki function. A deconvolution example for data obtained at 2 °C/min was shown in Fig. 8. The minor peaks before 200 °C and after 600 °C were likely related to light volatile release and vaporization of alkali salts (e.g., KCl and NaCl) or decomposition of carbonates, respectively [49,50], which were neglected during deconvolution. Table 3 summarized the fitting results. The Fraser-Suzuki deconvolution well fitted all curves at various heating rates with a fit error of 1.6–2.5%, indicating that the parallel reaction model can accurately predict the experimental data. The peak temperatures (P) for PC1 and PC2 at 10 °C/min were 346–354 °C and 445–456 °C, respectively, similar to deconvolution of manure digestate-derived hydrochar [51], which were attributed to the combustion of volatile matter and fixed carbon, respectively.

As shown in Fig. 8, at the same heating rate, modified hydrochar from a higher acid concentration had a smaller area of PC1 and a larger area of PC2, displaying a similar trend of dry ash-free volatile matter and fixed carbon, respectively (Fig. S3). A linear fitting found that the average relative area of PC1 and PC2 showed a strong positive correlation ($R^2 > 0.98$) to the content of volatile matter and fixed carbon, respectively (Fig. S5). This implies that modeled pseudo-components can reasonably represent the chemical composition of hydrochar,

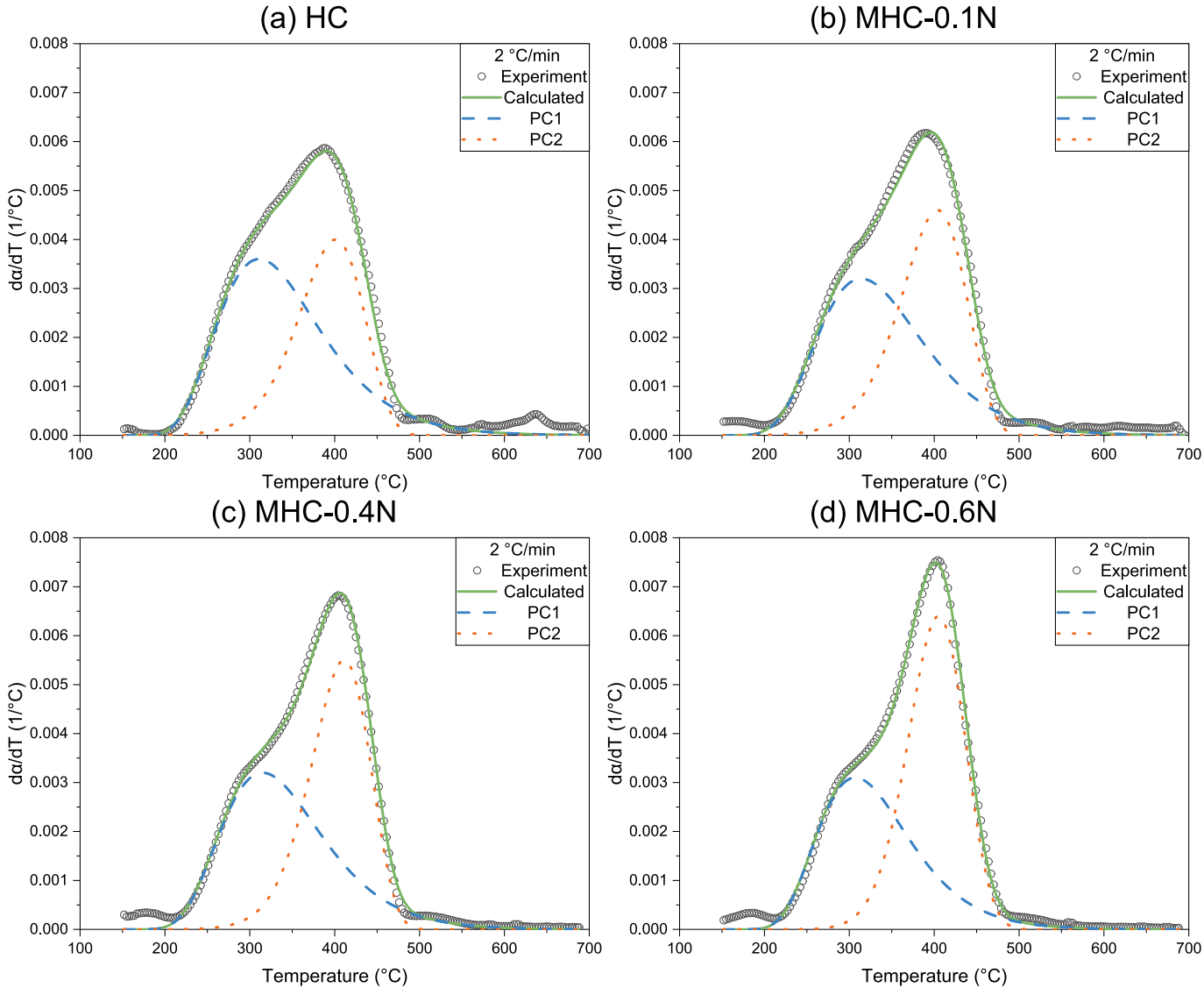

Fig. 8. Fraser-Suzuki deconvolution of reaction rates for combustion at 2 °C/min of (a) raw hydrochar (HC) and modified hydrochar (MHC) from an acid concentration of (b) 0.1 N, (c) 0.4 N, and (d) 0.6 N. PC1 – pseudo-component volatile matter, PC2 – pseudo-component fixed carbon.

Table 3
Fitting results of Fraser-Suzuki deconvolution for raw hydrochar (HC) and modified hydrochar (MHC).

Heating rate (°C/min)	Parameters	HC		MHC-0.1 N		MHC-0.4 N		MHC-0.6 N	
		PC1	PC2	PC1	PC2	PC1	PC2	PC1	PC2
2	H (1/°C)	0.0036	0.004	0.0032	0.0046	0.0032	0.0055	0.0031	0.0064
	P (°C)	311	401	314	404	315	411	307	405
	W (°C)	141	91	144	91	139	82	126	79
	A_s (−)	0.37	−0.25	0.34	−0.25	0.345	−0.23	0.345	−0.14
	Error (%)	2.42		2.23		1.72		1.63	
5	H (1/°C)	0.0033	0.0039	0.0031	0.0043	0.0028	0.0054	0.0028	0.0063
	P (°C)	333	427	337	429	337	436	328	432
	W (°C)	151	99	153	96	148	86	131	84
	A_s (−)	0.37	−0.25	0.34	−0.25	0.345	−0.23	0.35	−0.17
	Error (%)	2.41		2.15		2.12		1.89	
10	H (1/°C)	0.0032	0.0037	0.0029	0.004	0.0026	0.0052	0.0026	0.006
	P (°C)	350	445	353	446	354	456	346	450
	W (°C)	158	101	162	101	157	92	143	87
	A_s (−)	0.37	−0.25	0.34	−0.25	0.345	−0.23	0.345	−0.17
	Error (%)	2.49		2.34		2.22		2.42	

although they do not reflect the real contents.

Following the deconvolution, Friedman method was employed to estimate the E_α of each PC, and the reaction model for each PC was identified using the generalized master plot approach that is only valid for single-step kinetics. The high R^2 values (0.994–1.000) in Table S5 suggested a good linear fitting of Arrhenius plots in the conversion range

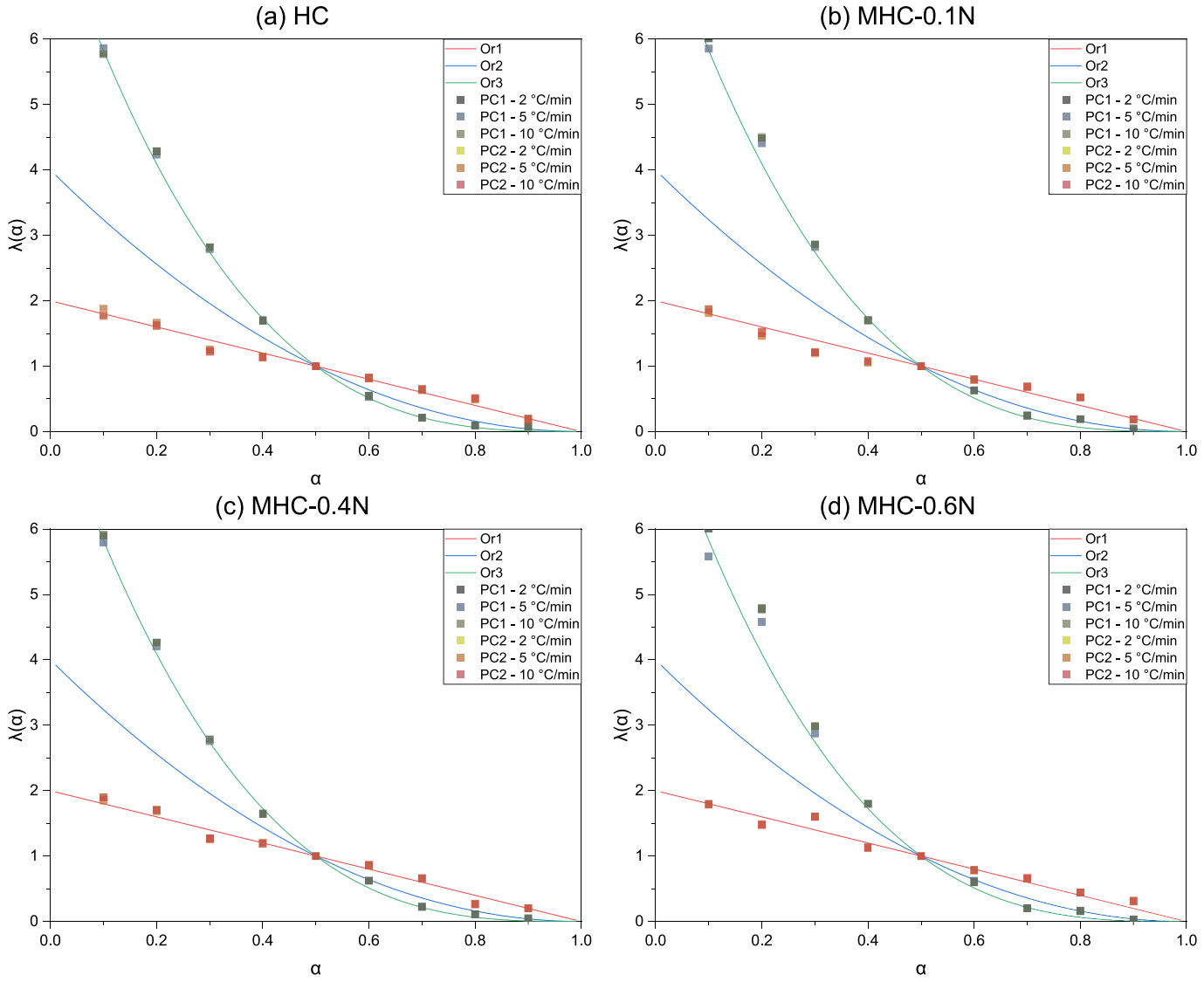

Fig. 9. Comparison between the experimental (scatter) and theoretical (line) master plots for pseudo-components (PC) of (a) raw hydrochar (HC) and modified hydrochar (MHC) by an acid concentration of (b) 0.1 N, (c) 0.4 N, and (d) 0.6 N. Orn – n^{th} order reaction model.

of 0.1–0.9 for each PC in all hydrochar. Using Eq. (12), λ(α) was calculated to construct the experimental master plots as a function of α for each PC at every heating rate. As shown in Fig. 9, experimental plots of PC1 and PC2 for all samples matched the theoretical master plot of third-order (Or3) and first-order (Or1) kinetic models, respectively. This means that the reaction rate of PC1 and PC2 is proportional to the cubic concentration and concentration of remaining components, respectively [52]. Notably, acidic leaching did not change the reaction mechanism or order, suggesting that chemical reaction is the rate-determining step for hydrochar combustion, which is likely controlled by principal reactants [53]. The identified combustion mechanism is similar to those previously reported. Using a double parallel reactions n^{th} order model, Wang et al. found that the first and second stages of biomass and coal combustion followed the order-based model with a reaction order of 2–4.5 and 0.8–1.5, respectively [44]. Assuming n^{th}-order reaction model, Sobek et al. deconvoluted four parallel reactions (n = 1–2) for the combustion of waste straw-derived hydrochar, while more steps were found probably due to the complex intermediates generated at a low hydrothermal temperature (250 °C) [19]. However, those studies only relied on model fitting without verifying the reaction model with the master plot method, which could mislead the actual mechanism. ICTAC has recommended that a model is only meaningful when it fits the data and gives kinetic or physical meaning [47]. Many previous studies assuming a first-order reaction were over-simplified and did not accurately describe the combustion of hydrochar. This study, for the first time, using combined deconvolution and master plot method, demonstrates that the combustion of hydrochar and MHC is controlled by two-step kinetics following n^{th} order reaction $f(\alpha) = (1 - \alpha)^n$ with varying reaction orders.

With the identification of reaction model, the frequency factor (A) for each PC could be calculated from the intercept of Eq. (6). The variations of E_α and ln(A) in terms of α were presented in Fig. 10 and their means of each PC in raw hydrochar and modified hydrochar were compared. Noticeably, E_α showed very limited dependence on α for both PCs, while E_α for PC1 increased towards the end of reaction ($\alpha > 0.7$) which was probably triggered by the latter reaction of PC2. The relative standard deviation of mean E_α for each PC was within 1–4%, always lower than those of mean E_α estimated by single-step kinetics (Fig. 7). The variations between the minimum and maximum E_α were $< 14\%$ and $< 6\%$ of the mean for PC1 and PC2, respectively. This indicates that multi-step kinetics can separate complex reactions and describe the combustion process of hydrochar better than treating it as a single step. Evidently, the overall E_α for PC1 (111–121 kJ/mol) was much lower than PC2 (139–143 kJ/mol), attributed to the lower thermal stability of volatile matter than fixed carbon.

Regarding the effects of acidic leaching, a low acid concentration (MHC-0.1 N) slightly enhanced E_α of PC1, while higher acid concentrations (MHC-0.4 N and MHC-0.6 N) significantly reduced E_α of PC1

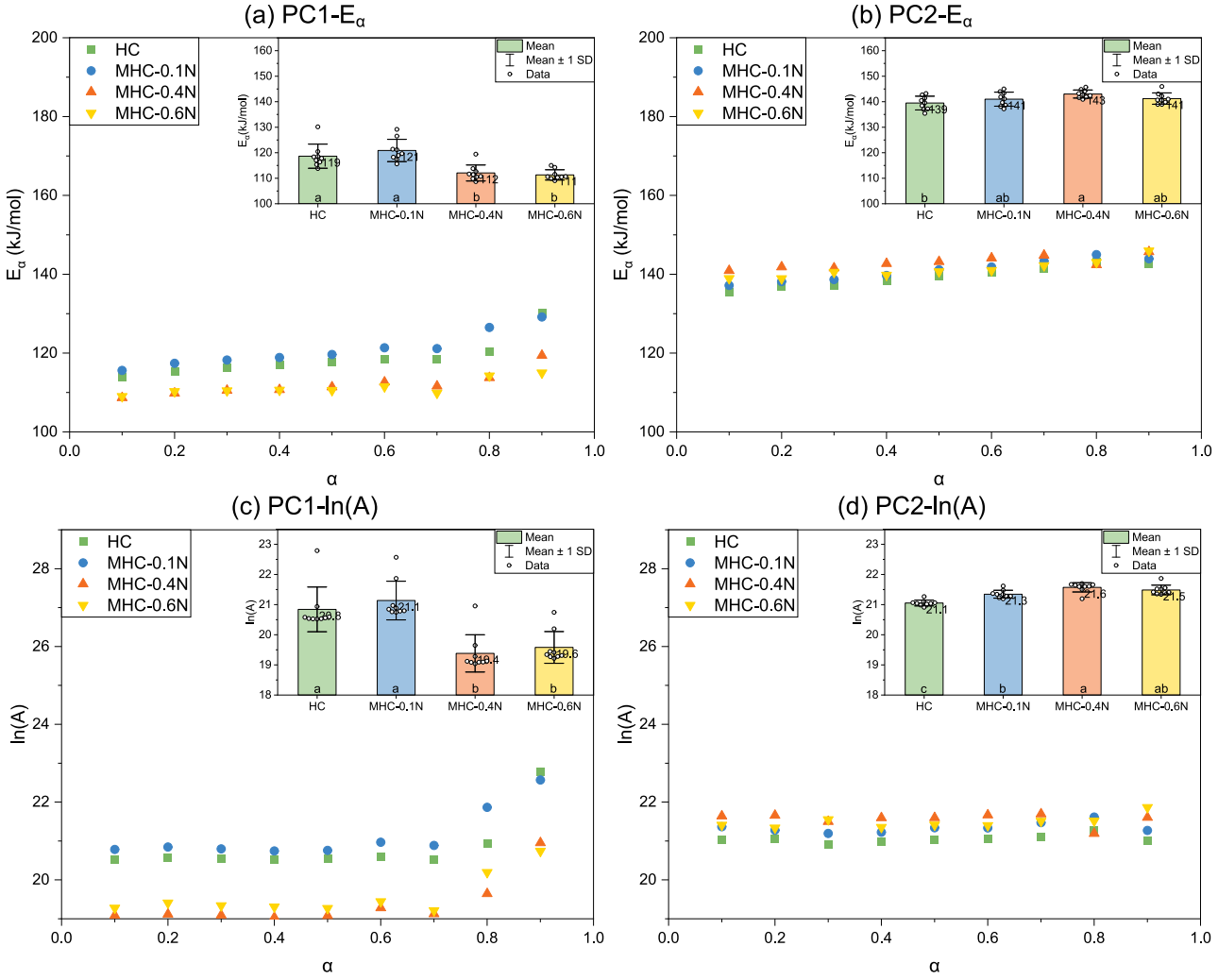

Fig. 10. Comparison of raw hydrochar (HC) and modified hydrochar (MHC) from different acid concentrations: (a-b) Apparent activation energy (E_α) and (c-d) frequency factor ln(A) for pseudo-components (PC). Inset shows a bar chart with mean ± standard deviation (SD). In each insert, columns that do not share a letter are significantly different ($p < 0.05$).

(Fig. 10a). The removal of easily reactive components (light volatiles) or catalytic metals (e.g., K, Ca, and Mg) by 0.1 N HNO_3 was probably responsible for the E_α increase [54]. On the other hand, stronger acid (0.4–0.6 N HNO_3) could improve the porous structure and surface area for air diffusion by removing ash, thus reducing E_α for PC1 [55]. For PC2, acidic modification did not show a significant impact on E_α although there was a slight increase for MHC-0.4 compared to HC (Fig. 10b). It was reported that devolatilization stage could reduce the E_α for the following step, while the increased O transfer rate by transition metal oxides (e.g., Fe_2O_3) could decrease E_α for fixed carbon combustion [43,44]. Therefore, the variation of E_α for PC2 could result from the combined effects of more volatile matter and fewer minerals due to acidic washing.

The pre-exponential factor (A) means the collision frequency of reactive molecules during decomposition. As a commonly found kinetic compensation effect (mutual correlation) between A and E_α [56], ln(A) showed similar changes to E_α in terms of α and acid modification (Fig. 10c-d). The relative standard deviations were at 2.6–4.5% and < 1% of mean ln(A) for PC1 and PC2, respectively. The calculated A (min^{-1}) values for PC1 were 1.12×10^9, 1.52×10^9, 2.61×10^8, and 3.19×10^8, and for PC2 were 1.39×10^9, 1.87×10^9, 2.33×10^9, and 2.15×10^9, respectively, in HC, MHC-0.1 N, MHC-0.4 N, and MHC-0.6 N, respectively. They were within the reported range (10^8–10^{16} min^{-1}) of bituminous coal [57].

4. Conclusion

This study demonstrated that after P recovery by acidic leaching, hydrochar showed significant improvements as a solid fuel, thus achieving zero waste for integrating HTL into WWTPs. The following remarks are concluded:

- The acidic leaching factors (L/S ratio, acid concentration, and contact time) all had significant effects on improving hydrochar fuel properties. The ash content was reduced by up to 44%, thus enhancing volatile matter, fixed carbon, fuel ratio, and HHV ratio by up to 1.2, 2.4, 2.2, and 1.7 times, respectively. Acidic leaching also increased CHN contents by 1.6 times while removing oxygenated compounds. The fuel properties of hydrochar can be maximized at the leaching conditions (10 mL/g of 0.6 N HNO_3 for 2 h) where most P was recovered.
- After acid washing, most minerals (e.g., Na_2O, CaO, MgO, Fe_2O_3, and P_2O_5) were removed and SiO_2 was concentrated in hydrochar. Such changes greatly reduced the slagging and fouling risks from high/severe to low in industrial boilers. Acidic leaching also improved the ignition temperature of hydrochar to 351 °C and the comprehensive combustion index to 9.9×10^{-8} min^{-2} $°C^{-3}$. Overall, MHC could achieve a fuel quality comparable to bituminous coal.
- The large variations of E_α estimated by single-step kinetics indicated that hydrochar combustion was controlled by multiple steps. Using Fraser-Suzuki deconvolution and master plot method, hydrochar combustion can be described by two-step kinetics. The pseudo-component volatile matter and fixed carbon all followed n^{th} order model $f(\alpha) = (1 - \alpha)^n$, with a reaction order of 3 and 1, respectively. Acidic leaching did not change the reaction order but significantly reduced the activation energy for the first stage while not affecting the second step much. The discovered reaction mechanism provides a fundamental reference for future research and design of combustors.

Declaration of Competing Interest

The authors declare that they have no known competing financial interests or personal relationships that could have appeared to influence the work reported in this paper.

Acknowledgments

This work was funded by the Natural Sciences and Engineering Research Council of Canada (NSERC) and Metro Vancouver Industrial Research Chair Program (IRCPJ 548816-18) in Advanced Resource Recovery from Wastewater; and NSERC Canada Graduate Scholarship – Doctoral program.

Appendix A. Supplementary data

Supplementary data to this article can be found online at https://doi.org/10.1016/j.cej.2023.145191.

References

[1] I.A. Basar, H. Liu, H. Carrere, E. Trably, C. Eskicioglu, A review on key design and operational parameters to optimize and develop hydrothermal liquefaction of biomass for biorefinery applications, Green Chem. 23 (2021) 1404–1446, https://doi.org/10.1039/D0GC04092D.
[2] H. Liu, I.A. Basar, A. Nzihou, C. Eskicioglu, Hydrochar derived from municipal sludge through hydrothermal processing: A critical review on its formation, characterization, and valorization, Water Res. 199 (2021), 117186, https://doi.org/10.1016/j.watres.2021.117186.
[3] I.A. Basar, H. Liu, C. Eskicioglu, Incorporating hydrothermal liquefaction into wastewater treatment – Part III: Aqueous phase characterization and evaluation of on-site treatment, Chem. Eng. J. 467 (2023), 143422, https://doi.org/10.1016/j.cej.2023.143422.
[4] K.K. Ramasamy, M.R. Thorson, J.M. Billing, J. Holladay, C. Drennan, B. Hoffman, Z. Haq, Hydrothermal Liquefaction : Path to Sustainable Aviation Fuel, 2021. https://www.osti.gov/biblio/1821809.
[5] P.A. Marrone, D.C. Elliott, J.M. Billing, R.T. Hallen, T.R. Hart, P. Kadota, J. C. Moeller, M.A. Randel, A.J. Schmidt, Bench-scale evaluation of hydrothermal processing technology for conversion of wastewater solids to fuels, Water Environ. Res. 90 (2018) 329–342, https://doi.org/10.2175/106143017x15131012152861.
[6] H. Liu, G. Hu, I.A. Basar, J. Li, N. Lyczko, A. Nzihou, C. Eskicioglu, Phosphorus recovery from municipal sludge-derived ash and hydrochar through wet-chemical technology: A review towards sustainable waste management, Chem. Eng. J. 417 (2021), 129300, https://doi.org/10.1016/j.cej.2021.129300.
[7] E. Ovsyannikova, A. Kruse, G.C. Becker, Feedstock-Dependent Phosphate Recovery in a Pilot-Scale Hydrothermal Liquefaction Bio-Crude Production, Energies. 13 (2020) 379, https://doi.org/10.3390/en13020379.
[8] H. Liu, N. Lyczko, A. Nzihou, C. Eskicioglu, Incorporating hydrothermal liquefaction into wastewater treatment – Part II: Characterization, environmental impacts, and potential applications of hydrochar, J. Clean. Prod. 383 (2023), 135398, https://doi.org/10.1016/j.jclepro.2022.135398.
[9] H. Liu, N. Lyczko, A. Nzihou, C. Eskicioglu, Phosphorus recovery from municipal sludge-derived hydrochar: Insights into leaching mechanisms and hydroxyapatite synthesis, Water Res. 241 (2023), 120138, https://doi.org/10.1016/j.watres.2023.120138.
[10] C. Nzediegwu, M.A. Naeth, S.X. Chang, Effects of nitric acid modification on hydrochar's combustion, fuel and thermal properties are dependent on feedstock type, Bioresour. Technol. 354 (2022), 127245, https://doi.org/10.1016/j.biortech.2022.127245.
[11] J. Lachman, M. Baláš, M. Lisý, H. Lisá, P. Milčák, P. Elbl, An overview of slagging and fouling indicators and their applicability to biomass fuels, Fuel Process. Technol. 217 (2021) 106804.
[12] J.D. Marin-Batista, A.F. Mohedano, J.J. Rodríguez, M.A. de la Rubia, Energy and phosphorous recovery through hydrothermal carbonization of digested sewage sludge, Waste Manag. 105 (2020) 566–574, https://doi.org/10.1016/j.wasman.2020.03.004.
[13] E. Song, S. Park, H. Kim, Upgrading hydrothermal carbonization (HTC) hydrochar from sewage sludge, Energies. 12 (2019) 2383, https://doi.org/10.3390/en12122383.
[14] Y. Zhang, Y. Guo, F. Cheng, K. Yan, Y. Cao, Investigation of combustion characteristics and kinetics of coal gangue with different feedstock properties by thermogravimetric analysis, Thermochim. Acta. 614 (2015) 137–148, https://doi.org/10.1016/j.tca.2015.06.018.
[15] M. Wilk, M. Śliz, B. Lubieniecki, Hydrothermal co-carbonization of sewage sludge and fuel additives: Combustion performance of hydrochar, Renew. Energy. 178 (2021) 1046–1056, https://doi.org/10.1016/j.renene.2021.06.101.
[16] Q. Wang, S. Wu, D. Cui, H. Zhou, D. Wu, S. Pan, F. Xu, Z. Wang, Co-hydrothermal carbonization of organic solid wastes to hydrochar as potential fuel: A review, Sci. Total Environ. 850 (2022), 158034, https://doi.org/10.1016/j.scitotenv.2022.158034.
[17] X. Zheng, J. Huang, Z. Ying, S. Ji, Y. Feng, B. Wang, B. Dou, Thermochemical conversion of sewage sludge-derived hydrochars: Volatiles release and char gasification kinetics, J. Anal. Appl. Pyrolysis. 156 (2021), 105138, https://doi.org/10.1016/j.jaap.2021.105138.
[18] Y. Li, H. Liu, K. Xiao, M. Jin, H. Xiao, H. Yao, Combustion and Pyrolysis Characteristics of Hydrochar Prepared by Hydrothermal Carbonization of Typical Food Waste: Influence of Carbohydrates, Proteins, and Lipids, Energy and Fuels. 34 (2020) 430–439, https://doi.org/10.1021/acs.energyfuels.9b02940.

[19] S. Sobek, Q.-K. Tran, R. Junga, S. Werle, Hydrothermal carbonization of the waste straw: A study of the biomass transient heating behavior and solid products combustion kinetics, Fuel. 314 (2022), 122725, https://doi.org/10.1016/j.fuel.2021.122725.

[20] H. Liu, I.A. Basar, C. Eskicioglu, Hydrothermal liquefaction for sludge-to-energy conversion: An evaluation of biocrude production and management of waste streams, Energy. 281 (2023), 128268, https://doi.org/10.1016/j.energy.2023.128268.

[21] D.P. Minh, P. Accart, C. Boachon, R. Calvet, A. Chesnaud, S. Del Confetto, J.L. Dirion, J. Dong, A. Ephraim, L. Haurie, N. Lyczko, R. Munirathinam, A. Nzihou, S. Patry, C. Rolland, L.M.R. Millán, L. Roques, A.R. Sane, R. Sani, E. Weiss-Hortala, C. E. White, Generic and advanced characterization techniques, in: Handb. Charact. Biomass, Biowaste Relat. By-Products, Springer, Cham, 2020: pp. 31–497. https://doi.org/10.1007/978-3-030-35020-8_2.

[22] R.W. Bryers, Fireside slagging, fouling, and high-temperature corrosion of heat-transfer surface due to impurities in steam-raising fuels, Prog. Energy Combust. Sci. 22 (1996) 29–120, https://doi.org/10.1016/0360-1285(95)00012-7.

[23] T.R. Miles, T.R.J. Miles, L.L. Baxter, R.W. Bryers, B.M. Jenkins, L.L. Oden, Alkali deposits found in biomass power plants: A preliminary investigation of their extent and nature. Volume 1, Washington, DC (United States), 1995. https://doi.org/10.2172/251288.

[24] F. Frandsen, Empirical Prediction of Ash Deposition Propensities in, Coal-Fired Utilities (1997). https://www.osti.gov/etdeweb/servlets/purl/594959.

[25] J.D. Singer, Combustion, fossil power systems: a reference book on fuel burning and steam generation, Third Edit, Combustion Engineering Inc., Windsor, CT (United States), 1981.

[26] M.T. Reza, J.G. Lynam, M.H. Uddin, C.J. Coronella, Hydrothermal carbonization: Fate of inorganics, Biomass Bioenergy. 49 (2013) 86–94, https://doi.org/10.1016/j.biombioe.2012.12.004.

[27] M. Pronobis, Evaluation of the influence of biomass co-combustion on boiler furnace slagging by means of fusibility correlations, Biomass Bioenergy. 28 (2005) 375–383, https://doi.org/10.1016/j.biombioe.2004.11.003.

[28] L.M. Romero Millán, F.E. Sierra Vargas, A. Nzihou, Kinetic Analysis of Tropical Lignocellulosic Agrowaste Pyrolysis, Bioenergy Res. 10 (2017) 832–845, https://doi.org/10.1007/s12155-017-9844-5.

[29] S. Vyazovkin, A.K. Burnham, J.M. Criado, L.A. Pérez-Maqueda, C. Popescu, N. Sbirrazzuoli, ICTAC Kinetics Committee recommendations for performing kinetic computations on thermal analysis data, Thermochim. Acta. 520 (2011) 1–19, https://doi.org/10.1016/j.tca.2011.03.034.

[30] M.J. Starink, The determination of activation energy from linear heating rate experiments: A comparison of the accuracy of isoconversion methods, Thermochim. Acta. 404 (2003) 163–176, https://doi.org/10.1016/S0040-6031(03)00144-8.

[31] L. Wang, Y. Chang, X. Zhang, F. Yang, Y. Li, X. Yang, S. Dong, Hydrothermal co-carbonization of sewage sludge and high concentration phenolic wastewater for production of solid biofuel with increased calorific value, J. Clean. Prod. 255 (2020) 120317.

[32] A. Perejón, P.E. Sánchez-Jiménez, J.M. Criado, L.A. Pérez-Maqueda, Kinetic analysis of complex solid-state reactions. A new deconvolution procedure, J. Phys. Chem. B. 115 (2011) 1780–1791, https://doi.org/10.1021/jp110895z.

[33] M. Wojdyr, Fityk: A general-purpose peak fitting program, J. Appl. Crystallogr. 43 (2010) 1126–1128, https://doi.org/10.1107/S0021889810030499.

[34] D.R. Nhuchhen, P. Abdul Salam, Estimation of higher heating value of biomass from proximate analysis: A new approach, Fuel. 99 (2012) 55–63, https://doi.org/10.1016/j.fuel.2012.04.015.

[35] R. Kurose, M. Ikeda, H. Makino, M. Kimoto, T. Miyazaki, Pulverized coal combustion characteristics of high-fuel-ratio coals, Fuel. 83 (2004) 1777–1785, https://doi.org/10.1016/j.fuel.2004.02.021.

[36] S. Bakshi, C. Banik, D.A. Laird, Estimating the organic oxygen content of biochar, Sci. Rep. 10 (2020) 1–12, https://doi.org/10.1038/s41598-020-69798-y.

[37] Y.H. Yu, C.M. Du, S.L. Fan, W.M. Yu, Acid-leaching separation of phosphorus from the BOF slag modified with Al2O3, J. Environ. Chem. Eng. 10 (2022) 108394. https://doi.org/10.1016/j.jece.2022.108394.

[38] M. Wang, D. Xu, Y. Bai, G. Yu, J. Zhang, S. Zhang, J. Xu, H. Zhang, S. Zhang, J. Wei, Dynamic investigation on potassium migration and transformation during biochar combustion and its correlation with combustion reactivity, Fuel. 340 (2023), 127540, https://doi.org/10.1016/j.fuel.2023.127540.

[39] T.A. Lasheen, Sulfate digestion process for high purity TiO2 from titania slag, Front. Chem. Eng. China. 3 (2009) 155–160, https://doi.org/10.1007/s11705-009-0005-z.

[40] A.M. Smith, S. Singh, A.B. Ross, Fate of inorganic material during hydrothermal carbonisation of biomass: Influence of feedstock on combustion behaviour of hydrochar, Fuel. 169 (2016) 135–145, https://doi.org/10.1016/j.fuel.2015.12.006.

[41] K.R. Parmar, A.B. Ross, Integration of hydrothermal carbonisation with anaerobic digestion; Opportunities for valorisation of digestate, Energies. 12 (9) (2019) 1586.

[42] J.J. Lu, W.H. Chen, Investigation on the ignition and burnout temperatures of bamboo and sugarcane bagasse by thermogravimetric analysis, Appl. Energy. 160 (2015) 49–57, https://doi.org/10.1016/j.apenergy.2015.09.026.

[43] Y. Wang, L. Jia, B. Guo, B. Wang, L. Zhang, X. Zheng, J. Xiang, Y. Jin, Effects of CaO-Fe2O3-Fe3(PO4)2 in sewage sludge on combustion characteristics and kinetics of coal slime, Fuel. 322 (2022), 124267, https://doi.org/10.1016/j.fuel.2022.124267.

[44] G. Wang, J. Zhang, J. Shao, Z. Liu, G. Zhang, T. Xu, J. Guo, H. Wang, R. Xu, H. Lin, Thermal behavior and kinetic analysis of co-combustion of waste biomass/low rank coal blends, Energy Convers. Manag. 124 (2016) 414–426, https://doi.org/10.1016/j.enconman.2016.07.045.

[45] F. Guo, Y. He, A. Hassanpour, J. Gardy, Z. Zhong, Thermogravimetric analysis on the co-combustion of biomass pellets with lignite and bituminous coal, Energy. 197 (2020), 117147, https://doi.org/10.1016/j.energy.2020.117147.

[46] K. Wang, T. Han, J. Deng, Y. Zhang, Comparison of combustion characteristics and kinetics of Jurassic and Carboniferous-Permian coals in China, Energy. 254 (2022), 124315, https://doi.org/10.1016/j.energy.2022.124315.

[47] S. Vyazovkin, A.K. Burnham, L. Favergeon, N. Koga, E. Moukhina, L.A. Pérez-Maqueda, N. Sbirrazzuoli, ICTAC Kinetics Committee recommendations for analysis of multi-step kinetics, Thermochim. Acta. 689 (2020), 178597, https://doi.org/10.1016/j.tca.2020.178597.

[48] T. Liu, Q. Lang, Y. Xia, Z. Chen, D. Li, J. Ma, C. Gai, Z. Liu, Combination of hydrothermal carbonization and oxy-fuel combustion process for sewage sludge treatment: Combustion characteristics and kinetics analysis, Fuel. 242 (2019) 265–276, https://doi.org/10.1016/j.fuel.2019.01.035.

[49] W. Jerzak, M. Kuźnia, Examination of inorganic gaseous species and condensed phases during coconut husk combustion based on thermodynamic equilibrium predictions, Renew. Energy. 167 (2021) 497–507, https://doi.org/10.1016/j.renene.2020.11.105.

[50] W. Yang, D. Pudasainee, R. Gupta, W. Li, B. Wang, L. Sun, An overview of inorganic particulate matter emission from coal/biomass/MSW combustion: Sampling and measurement, formation, distribution, inorganic composition and influencing factors, Fuel Process. Technol. 213 (2021), 106657, https://doi.org/10.1016/J.FUPROC.2020.106657.

[51] V. Benedetti, M. Pecchi, M. Baratieri, Combustion kinetics of hydrochar from cow-manure digestate via thermogravimetric analysis and peak deconvolution, Bioresour. Technol. 353 (2022), 127142, https://doi.org/10.1016/j.biortech.2022.127142.

[52] S. Niu, M. Chen, Y. Li, J. Song, Co-combustion characteristics of municipal sewage sludge and bituminous coal, J. Therm. Anal. Calorim. 131 (2018) 1821–1834, https://doi.org/10.1007/s10973-017-6716-3.

[53] E.C. Moine, M. Tangarfa, M. Khachani, A. El Hamidi, M. Halim, S. Arsalane, Thermal oxidation study of Moroccan oil shale: A new approach to non-isothermal kinetics based on deconvolution procedure, Fuel. 180 (2016) 529–537, https://doi.org/10.1016/j.fuel.2016.04.076.

[54] J. Cai, S. Wang, C. Kuang, X. Tang, Insight into the kinetic analysis of catalytic combustion for biomass after alkaline metals loaded pretreatment, Fuel. 203 (2017) 501–513, https://doi.org/10.1016/j.fuel.2017.04.137.

[55] X. Dong, S. Guo, M. Ma, H. Zheng, X. Gao, S. Wang, H. Zhang, Hydrothermal carbonization of millet stalk and dilute-acid-impregnated millet stalk: combustion behaviors of hydrochars by thermogravimetric analysis and a novel mixed-function fitting method, Fuel. 273 (2020), 117734, https://doi.org/10.1016/j.fuel.2020.117734.

[56] N. Koga, S. Vyazovkin, A.K. Burnham, L. Favergeon, N.V. Muravyev, L.A. Pérez-Maqueda, C. Saggese, P.E. Sánchez-Jiménez, ICTAC Kinetics Committee recommendations for analysis of thermal decomposition kinetics, Thermochim. Acta. 719 (2023) 179384.

[57] C. Zou, L. Zhang, S. Cao, C. Zheng, A study of combustion characteristics of pulverized coal in O2/H2O atmosphere, Fuel. 115 (2014) 312–320, https://doi.org/10.1016/j.fuel.2013.07.025.